

Calcium channel dynamics limit synaptic release in response to prosthetic stimulation with sinusoidal waveforms

This article has been downloaded from IOPscience. Please scroll down to see the full text article.

2011 J. Neural Eng. 8 046005

(<http://iopscience.iop.org/1741-2552/8/4/046005>)

View [the table of contents for this issue](#), or go to the [journal homepage](#) for more

Download details:

IP Address: 18.7.29.240

The article was downloaded on 14/09/2011 at 17:06

Please note that [terms and conditions apply](#).

Calcium channel dynamics limit synaptic release in response to prosthetic stimulation with sinusoidal waveforms

Daniel K Freeman^{1,2}, Jed S Jeng^{1,2}, Shawn K Kelly^{1,3}, Espen Hartveit⁴
and Shelley I Fried^{1,2}

¹ Center for Innovative Visual Rehabilitation, Boston VA Healthcare System, 150 South Huntington Ave, Boston, MA 02130, USA

² Department of Neurosurgery, Massachusetts General Hospital and Harvard Medical School, 165 Cambridge Street, Boston, MA 02114, USA

³ Research Laboratory of Electronics, Massachusetts Institute of Technology, 77 Massachusetts Ave, Cambridge, MA 02139, USA

⁴ Department of Biomedicine, University of Bergen, Jonas Lies vei 91, N-5009 Bergen, Norway

E-mail: fried.shelley@mg.harvard.edu

Received 22 February 2011

Accepted for publication 19 April 2011

Published 31 May 2011

Online at stacks.iop.org/JNE/8/046005

Abstract

Extracellular electric stimulation with sinusoidal waveforms has been shown to allow preferential activation of individual types of retinal neurons by varying stimulus frequency. It is important to understand the mechanisms underlying this frequency dependence as a step toward improving methods of preferential activation. In order to elucidate these mechanisms, we implemented a morphologically realistic model of a retinal bipolar cell and measured the response to extracellular stimulation with sinusoidal waveforms. We compared the frequency response of a passive membrane model to the kinetics of voltage-gated calcium channels that mediate synaptic release. The passive electrical properties of the membrane exhibited lowpass filtering with a relatively high cutoff frequency (nominal value = 717 Hz). This cutoff frequency was dependent on intra-axonal resistance, with shorter and wider axons yielding higher cutoff frequencies. However, we found that the cutoff frequency of bipolar cell synaptic release was primarily limited by the relatively slow opening kinetics of L- and T-type calcium channels. The cutoff frequency of calcium currents depended nonlinearly on stimulus amplitude, but remained lower than the cutoff frequency of the passive membrane model for a large range of membrane potential fluctuations. These results suggest that while it may be possible to modulate the membrane potential of bipolar cells over a wide range of stimulus frequencies, synaptic release will only be initiated at the lower end of this range.

 Online supplementary data available from stacks.iop.org/JNE/8/046005/mmedia

Introduction

Diseases of the outer retina such as macular degeneration and retinitis pigmentosa result in degeneration of the photoreceptors, the neurons primarily responsible for sensing light. However, many neurons in the inner retina, including bipolar and ganglion cells, remain viable (Strettoi *et al* 2003, Margolis *et al* 2008, Mazzoni *et al* 2008). Much effort has been devoted to exploring whether vision can be partially restored

by electrically stimulating surviving neurons with a retinal prosthetic (Zrenner 2002, Weiland *et al* 2004, Winter *et al* 2007). Human trials have shown some success (Rizzo *et al* 2003, Ahuja *et al* 2010, Zrenner *et al* 2010), but the quality of elicited vision must be improved in order for such devices to significantly affect quality of life (Chader *et al* 2009).

One of the obstacles to improving the quality of vision with retinal prostheses is thought to be the inability to control the spatial and temporal pattern of elicited ganglion cell spike

trains (for a review, see Freeman *et al* (2011)). The manner in which ganglion cells encode visual information under normal physiological conditions is thought to be complex (Field and Chichilnisky 2007, Gollisch and Meister 2010), suggesting that sophisticated stimulation methods may be needed to replicate such spiking patterns. Using electric stimulation, spiking can be elicited in the ganglion cells in two ways: (1) via direct activation of the ganglion cell, or (2) indirectly, by activating presynaptic neurons (e.g. bipolar cells) and thereby altering the levels of synaptic release onto the ganglion cells (Jensen *et al* 2005a, Fried *et al* 2006, Margalit and Thoreson 2006, Sekirnjak *et al* 2006, Freeman and Fried 2011). However, the ability to selectively or even preferentially activate the direct versus indirect response is limited using stimulation with pulse trains ((Jensen *et al* 2005b, Fried *et al* 2006, Tsai *et al* 2009) but see (Stett *et al* 2007)).

Recent evidence suggests that alternative stimulus waveforms may offer advantages over pulse trains for producing selective activation. For example, Freeman *et al* (2010) found that stimulation with low-frequency sinusoids (5–25 Hz) produced a robust response through indirect activation, but produced little or no response through direct activation of the ganglion cell. The ability of low-frequency sinusoids to preferentially activate the indirect response may be advantageous in allowing existing inner retinal circuitry to be utilized, presumably resulting in spike trains that better resemble those that are present in the healthy retina. In addition, low-frequency sinusoids avoid the activation of passing axons; this is thought to be critical for generating spatially focal percepts.

The mechanisms underlying the preferential activation of the indirect response at low stimulus frequencies remain unresolved. There are at least three major factors that influence the neuronal response to electric stimulation, each of which may contribute to the observed frequency dependence. First, the membrane potential will be altered by the direct action of the electric stimulus on the targeted neuron; the magnitude and timing of any changes in membrane potential will depend on the passive electrical properties of the neuron (e.g. the resistance and capacitance of the cell membrane) (Rattay 1998, Gerhardt *et al* 2010). Second, changes in membrane potential will alter the flow of current through voltage-gated ion channels (McIntyre and Grill 1998, Greenberg *et al* 1999, Boinagrov *et al* 2010); the magnitude and timing of these currents will depend on the gating kinetics of the associated ion channel. Third, modulations in the level of excitatory and/or inhibitory input can occur if presynaptic neurons are also activated by stimulation (Fried *et al* 2006, Margalit and Thoreson 2006).

Here, we examined the contribution of the passive membrane properties and voltage-gated calcium channels of bipolar cells to the preferential activation of the indirect response at low frequencies. These two mechanisms are both intrinsic to the bipolar cell, while the influence of neurons that are presynaptic to the bipolar cell (i.e. photoreceptors and amacrine cells) were considered extrinsic effects and were excluded from this study. Previous work has raised the possibility that both intrinsic mechanisms described

above could contribute to the preferential activation seen physiologically. For example, a recent modeling study found that the passive membrane properties of bipolar cells may act to lowpass filter the applied stimulus (Gerhardt *et al* 2010). This suggests that membrane potential is modulated more strongly at low stimulus frequencies. In addition, while several different types of voltage-gated ion channels have been identified in bipolar cells (Ma *et al* 2005), calcium entry into the axon terminals through L- and T-type calcium channels is known to underlie synaptic release (Tachibana *et al* 1993, Pan *et al* 2001). Because these channels have relatively slow opening kinetics (Pan 2000, Pan *et al* 2001), it is possible that calcium influx is stronger at low stimulus frequencies than high frequencies (even though the membrane potential of bipolar cells is modulated equally at both low and high stimulus frequencies).

To distinguish between these possibilities, we built a series of computational models that allowed us to assess the contribution of each factor in isolation. We found that the passive membrane properties of the bipolar cell did not influence the response for frequencies below several hundred hertz (cutoff frequency of 717 Hz for a ‘typical’ bipolar cell). In contrast, calcium channels responded maximally to relatively low stimulus frequencies (peak frequency of 5–25 Hz for T-type channels, and cutoff frequency of 65–500 Hz for L-type channels). Thus, our results suggest that the slow kinetics of calcium channels and not the passive membrane properties limit synaptic release in response to sinusoidal electric stimulation.

Methods

Two-compartment model

Retinal bipolar cells receive synaptic input from photoreceptors in the outer retina and provide synaptic input to amacrine and ganglion cells in the inner retina. Under normal physiological conditions, fluctuations in membrane potential at the soma propagate passively down the axon to the axon terminals (e.g. no spiking) (figure 1(A)), where synaptic release is initiated. We implemented a two-compartment model of a bipolar cell modified from previous work (Mennerick *et al* 1997, Oltedal *et al* 2007). The soma and terminals were each represented by a single compartment that contained a resistor and capacitor in parallel (figure 1(B)). The two compartments were connected by a single resistor (R_{axon}), representing resistance to current flow along the inside of the axon. Extracellular stimulation was modeled as a voltage source applied across the soma and terminal regions (V_{stim}). This was based on a common model of extracellular stimulation where a spatial gradient in voltage along the outside of the cell causes current to flow through and along the cell membrane (McNeal 1976). Because synaptic release is mediated by calcium entry through voltage-gated channels in the synaptic terminals, we were interested in how the membrane potential in the terminals (V_{term}) varied in response to sinusoidal modulations of V_{stim} . The motivation for using this simple two-compartment model is that it

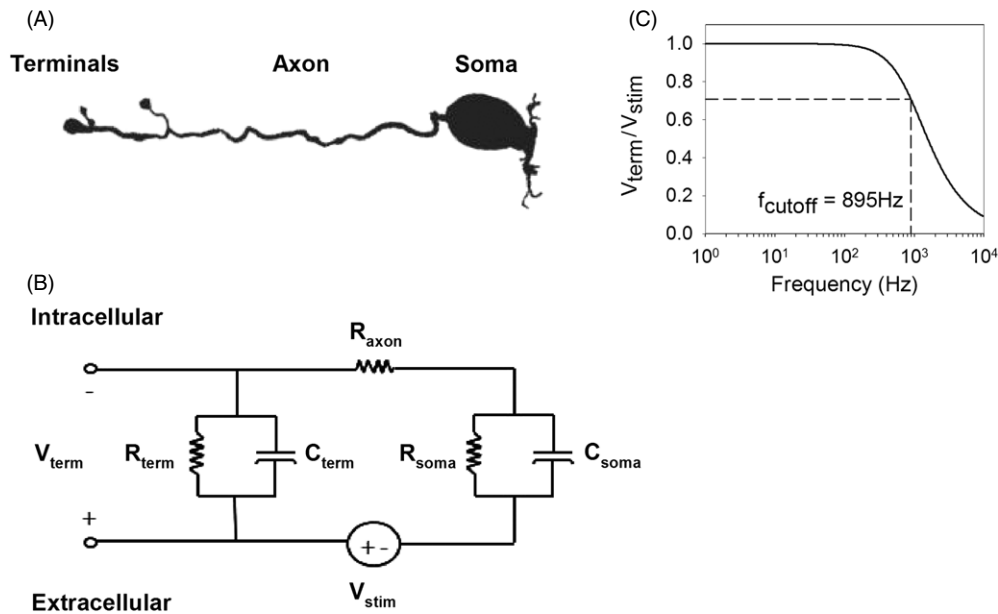


Figure 1. Two-compartment, passive model of a bipolar cell. (A) Morphological reconstruction of a rod bipolar cell illustrating the soma, axon and terminal regions. (B) Schematic of the two-compartment model. The soma and terminal regions are each represented by a resistor and capacitor in parallel. The resistance to intra-axonal current flow is represented by a resistor (R_{axon}). The stimulus is represented by a voltage applied extracellularly across the soma and terminal compartments (V_{stim}). (C) The transfer function (V_{term}/V_{stim}) was normalized and plotted versus stimulus frequency, where V_{term} represents the membrane potential at the terminal compartment. The cutoff frequency (895 Hz) was defined as the frequency at which V_{term}/V_{stim} was reduced to 3 dB. The nominal values of the circuit elements were $R_{soma} = 5.98 \text{ G}\Omega$, $C_{soma} = 3.7 \text{ pF}$, $R_{term} = 27.9 \text{ G}\Omega$, $C_{term} = 0.8 \text{ pF}$, $R_{axon} = 272.2 \text{ M}\Omega$.

allows linear circuit analysis to be used to derive a direct mathematical relationship between the applied stimulus (V_{stim}) and the membrane potential in the terminals (V_{term}). Analysis was performed using Matlab software (Mathworks, Natick, MA).

Multi-compartment model

In addition to the two-compartment model, we implemented a multi-compartment bipolar cell model developed in previous work (figures 4(A) and (B)) (Oltedal *et al* 2009, Oltedal and Hartveit 2010). This model was based on the morphologically reconstructed rod bipolar cell shown in figure 1(A), and contained a total of 92 compartments (Oltedal *et al* 2009). The model was implemented in the NEURON (Hines 1993) simulation environment and modified to include the effects of extracellular electric stimulation. As with previous work implementing extracellular stimulation of a model neuron (Greenberg *et al* 1999), an ideal monopolar point source was used to represent the stimulating electrode. The point source was positioned $40 \mu\text{m}$ from the terminals (i.e. $40 \mu\text{m}$ from the leftmost point of the cell in figure 4(A)), unless stated otherwise. The external medium in which the current travels was assumed to be homogeneous and infinite. The extracellular potential at each point in space is related instantaneously to the applied stimulus voltage, where extracellular potential falls inversely with distance from the point of stimulation according to the following equation:

$$V_e = (\rho_e I_{stim}) / (4 \pi r)$$

where V_e is the extracellular potential, I_{stim} is the amplitude of the stimulus, ρ_e is the resistivity of the extracellular

medium (set to $110 \Omega \text{ cm}$) (Coleman and Miller 1989), and r is the distance between the stimulating electrode and the center of each compartment. For each simulation, the extracellular voltage for each compartment was modulated sinusoidally and the resulting membrane potential of each compartment was determined. Non-uniformities in the electric field arising from the presence of the model cell were ignored.

Parameter values

For the multi-compartment model, the cell was considered to be of three sections: the soma, axon and terminals. Dendrites arising from the soma were considered as part of the soma section and were not modeled separately. The following parameter values were derived from the multi-compartment model in Oltedal *et al* (2009). The axon length was $39.6 \mu\text{m}$, as measured from the soma to the first bifurcation, beyond which was considered the terminals. The axonal diameter, averaged across the length of the axon, was $0.71 \mu\text{m}$. The specific membrane capacitance (C_m) was set to $1.07 \mu\text{F cm}^{-2}$, the specific membrane conductance (g_{leak}) was set to $48.00 \mu\text{S cm}^{-2}$ and the leak reversal potential (E_{leak}) was set to -50 mV . For a given compartment, the leak conductance and membrane capacitance were determined by scaling the specific membrane conductance and capacitance by the surface area of the membrane. The resistance to current flow along the length of the cell was modeled with a resistor connecting each compartment within the interior of the cell. For consistency, this resistor was quantified in terms of conductance (g_{intra}), and not resistance; g_{intra}

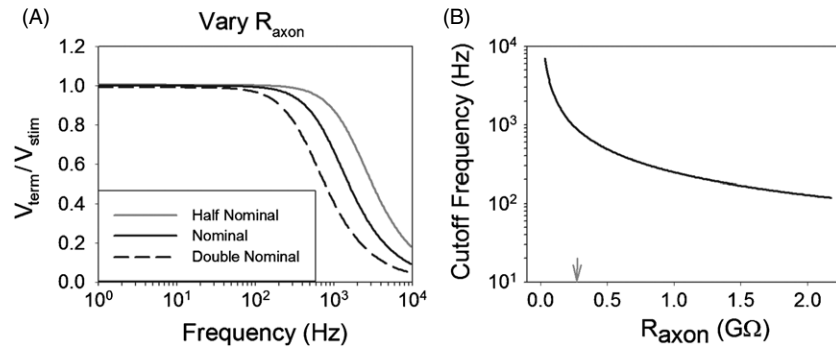


Figure 2. Changes to axonal resistance alter the cutoff frequency. (A) The transfer function of the two-compartment model is shown for the nominal value of R_{axon} (272.2 M Ω), as well as for one-half and double this value. The nominal curve was normalized to unity and the other curves are scaled relative to this value. (B) The cutoff frequency is plotted for values of R_{axon} ranging from 1/8 to 8 \times nominal; the arrow indicates the nominal value.

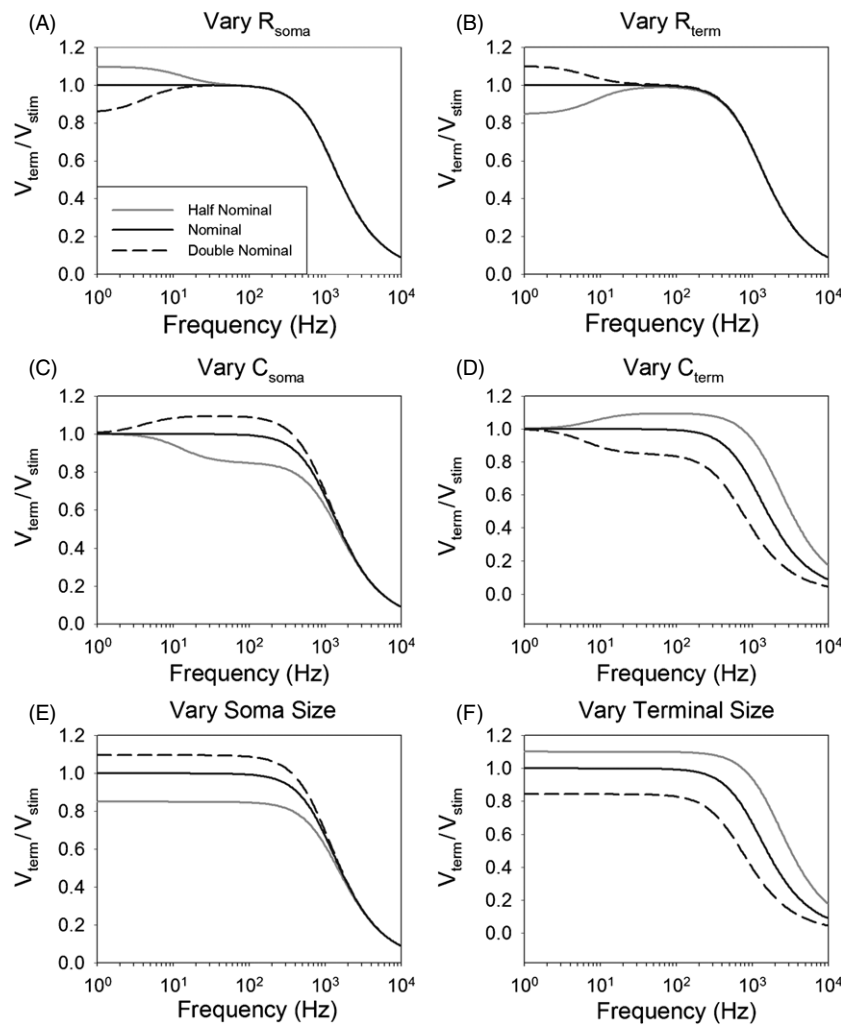


Figure 3. Effect of varying the resistance and capacitance of the soma and terminal compartments on the transfer function of the two-compartment model. The effect of varying R_{soma} (A), R_{term} (B), C_{soma} (C) and C_{term} (D) on the transfer function. Variations in the size of the soma (E) and terminals (F) were simulated by varying resistance and capacitance simultaneously (see the text). For all plots, the nominal curve was normalized to unity and the other curves were scaled relative to this value (see the Methods section). The legend in panel A applies to all plots.

was computed as a function of intra-cellular resistivity ($\rho_i = 189.6 \Omega \text{ cm}$, unless stated otherwise), the cross-sectional area of the cell and the length of each compartment.

For the two-compartment model, the nominal values of the resistors and capacitors in the soma and terminals were derived from values in the multi-compartment model

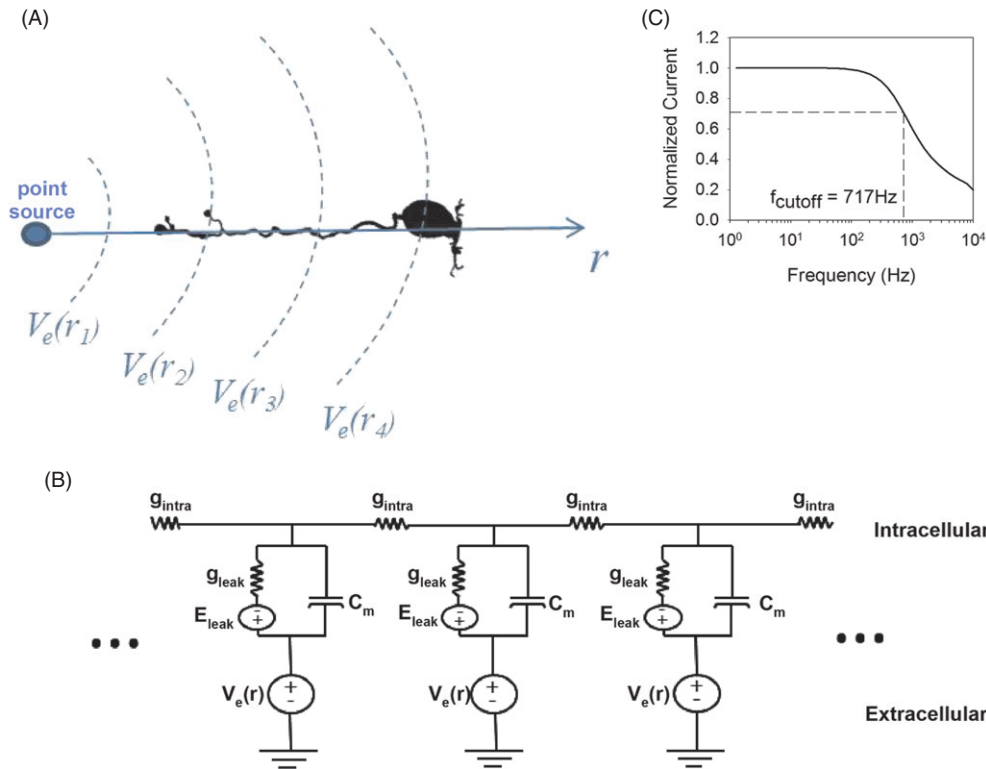


Figure 4. Multi-compartment, passive model of a bipolar cell. (A) The stimulus is represented by a point source that was positioned $40 \mu\text{m}$ from the terminals. During stimulation, the extracellular voltage (V_e) is computed as a function of the distance r , from the point source. (B) Schematic of the multi-compartment model. Each compartment contains a resistor and capacitor in parallel, representing the leak conductance (g_{leak}) and membrane capacitance (C_m), respectively. Intracellular current flow between neighboring compartments is represented by the conductance g_{intra} . (C) The frequency response was measured by sinusoidally modulating $V_e(r)$ and measuring the resulting membrane potential in the terminals (V_{term}). Nominal membrane parameters were $C_m = 1.07 \mu\text{F cm}^{-2}$, $g_{leak} = 48.00 \mu\text{S cm}^{-2}$, and $\rho_i = 189.6 \Omega \text{ cm}$.

(This figure is in colour only in the electronic version)

by scaling specific membrane conductance ($48.0 \mu\text{S cm}^{-2}$) and capacitance ($1.07 \mu\text{F cm}^{-2}$) to the area of the soma ($348.3 \mu\text{m}^2$) and terminal ($74.7 \mu\text{m}^2$) regions. The resulting values of the resistors and capacitors were $R_{soma} = 5.98 \text{ G}\Omega$, $C_{soma} = 3.7 \text{ pF}$, $R_{term} = 27.9 \text{ G}\Omega$, and $C_{term} = 0.8 \text{ pF}$. The axonal resistance was computed by summing up the intra-axonal resistance along the length of the multi-compartment neuron, giving a value of $R_{axon} = 272.2 \text{ M}\Omega$.

The anatomical properties of bipolar cells can vary considerably across approximately ten types of bipolar cells (Euler and Wässle 1995, Boycott and Wässle 1999, Wu *et al* 2000). We were interested in understanding the sensitivity of the model to changes in bipolar cell anatomy, including variations in axonal length and diameter, as well as soma and terminal size. This required us to define a range of values over which each parameter was varied. For example, axonal length varies from 10 to $50 \mu\text{m}$ across bipolar cell types (Euler and Wässle 1995, Ghosh *et al* 2004), and other anatomical parameters, such as soma and terminal size, can vary considerably across species even in cells of the same type (Camino *et al* 2000). Therefore, instead of trying to replicate the precise range of configurations seen across species and across bipolar cell types within a given species, we chose to increase and decrease each parameter by a factor of 2 from nominal ($39.6 \mu\text{m}$) (total range of a factor of 4), thereby

allowing the general characterization of the sensitivity of the model to each parameter.

Calcium channel simulations

Current flowing through L- and T-type calcium channels and into the cell initiates synaptic release from bipolar cell terminals (Tachibana *et al* 1993, Pan *et al* 2001). As a result, the dynamics of the opening/closing of L- and T-type channels in response to changes in membrane potential may play an important role in shaping the frequency response of synaptic release in response to extracellular stimulation. Therefore, we examined the gating equations for L- and T-type channels in order to investigate their contribution to the bipolar cell response independent from the effects of the passive membrane properties of the neuron.

Equations describing the voltage dependence of these channels have not been reported in bipolar cells. Therefore, we used equations for the L-type calcium channel derived from work in retinal ganglion cells (Benison *et al* 2001). This model was chosen because it exhibited similar response kinetics and threshold for activation as the physiologically reported L-type currents in bipolar cells (Tachibana *et al* 1993, von Gersdorff and Matthews 1996, Hartveit 1999, Hu *et al* 2009). For T-type channels, we implemented a model

based on cerebellar Purkinje neurons (De Schutter and Bower 1994); these channels exhibited a relatively low threshold for activation that is characteristic of T-type currents reported from physiological studies on bipolar cells (Kaneko *et al* 1989, Hu *et al* 2009). In order to test whether the results were specific to the choice of model, we also simulated other model equations for L-type (McCormick and Huguenard 1992) and T-type (Huguenard and McCormick 1992) channels based on thalamic relay neurons (see supplementary material available at stacks.iop.org/JNE/8/046005/mmedia).

We simulated these equations in voltage-clamp conditions in which the voltage was varied sinusoidally and the resulting calcium current was measured. The voltage was oscillated about a baseline level of -50 mV; this value is approximately midway between the reported resting membrane potential of cone bipolar cells (-57.6 mV) and rod bipolar cells (-45.4 mV) (Ma *et al* 2005). The maximal fluctuation in bipolar cell membrane potential elicited by electric stimulation is unknown. Therefore, we tested over a wide range of voltage fluctuations, ranging from 2.5 to 100 mV (i.e. reaching depolarization levels of -47.5 to $+50$ mV). The L-type currents (I_L) and the T-type currents (I_T) were computed as follows:

$$I_L = g_L(V - E_{Ca})$$

$$I_T = g_T(V - E_{Ca}).$$

The conductance of each channel was nonlinear, defined as

$$g_L = g_{Lmax} m^2$$

$$g_T = g_{Tmax} n h$$

where $E_{Ca} = 45$ mV, $g_{Lmax} = g_{Tmax} = g_{leak} = 48.0 \mu S cm^{-2}$, and m , n and h are defined below. Note that the magnitude of g_{Lmax} and g_{Tmax} will not affect the shape of the frequency responses and will only scale the magnitudes of the resulting currents.

The relationship between voltage and channel conductance was based on the formalism of Hodgkin and Huxley (1952):

$$\frac{dp}{dt} = \alpha_p(V) (1 - p) - \beta_p(V) p$$

where $p = m$, n and h . The gating parameters m and n are activating (open in response to depolarization), and the parameter h is inactivating (open in response to hyperpolarization). The voltage-dependent equations $\alpha_p(V)$ and $\beta_p(V)$ can be found in the original articles (De Schutter and Bower 1994, Benison *et al* 2001). Differential equations were solved in Matlab using Euler's method with a timestep of 0.01–0.1 ms. The resulting currents were measured as peak to peak.

Incorporating calcium channels into the multi-compartment model

Following the analysis of the multi-compartment model with only passive membrane elements, L- and T-type calcium channels were added to the terminal region of the bipolar cell in parallel with the leak conductance. The current through these channels was measured in response to sinusoidal extracellular stimulation. Since the release of synaptic vesicles results from

the influx of calcium to the cell, the amount of current through the calcium channels was interpreted as a measure of synaptic release from the bipolar cell in response to electric stimulation.

The total membrane conductance of either L- or T-type calcium channels in bipolar cells has not been reported. We set the maximum membrane conductance for L- and T-type calcium channels (g_{Lmax} and g_{Tmax}) to be equal to the leak conductance ($g_{leak} = g_{Lmax} = g_{Tmax}$). The reason for this was that if the calcium conductance was set larger than the leak, then a regenerative response could occur where all calcium channels open and remain open; such behavior is not thought to occur under normal physiological conditions (see also the Discussion section 'Effects of calcium conductance and other voltage-gated ion channels').

Normalization procedures

For the two-compartment model, an analytical expression was derived for the transfer function, defined as V_{term}/V_{stim} . However, the transfer function of the multi-compartment model, defined as V_{term}/I_{stim} , was too complex to express analytically, and therefore the frequency response was obtained by measuring V_{term} in response to sinusoidal modulations of I_{stim} as a function of stimulus frequency. The normalization procedure for the frequency response (or transfer function) contained two steps. First, the frequency response (or transfer function) obtained for nominal model parameters was normalized to unity (figures 1(C) and 4(C)). Second, the frequency response (or transfer function) obtained for other model parameters was normalized by the same factor in order to allow direct comparison to nominal curves (e.g. figure 3(A)). Note that for two-compartment and multi-compartment passive models (i.e. when no calcium channels were present), the circuit contained only linear elements. Therefore, the shape of the frequency response was not dependent on stimulus amplitude, and was obtained only for a single stimulus amplitude. In some instances, all curves in a given plot were normalized to unity to allow comparison; in these cases the axes were labeled as 'normalized' (e.g. figure 7(B)). Cutoff frequency is defined as the frequency at which the response is decreased from maximum by 3 dB ($1/\sqrt{2}$, or 0.707 of maximum).

Results

Previous work indicates that in response to sinusoidal electric stimulation delivered from an extracellular electrode, bipolar cell synaptic output is stronger in response to low frequencies (10–25 Hz) as compared to high frequencies (100 Hz) (Freeman *et al* 2010). In order to elucidate the mechanisms underlying this frequency dependence, we examined the contribution of passive electrical properties (i.e. no voltage-gated channels) of the bipolar cell membrane to the frequency response using two approaches. First, the bipolar cell was represented by a two-compartment model. The simplicity of this model allowed the transfer function to be derived analytically using linear circuit analysis. Second, a morphologically realistic multi-compartment model

was implemented in order to account for the complex morphological structure of a bipolar cell. Then, after the contribution of the passive electrical properties to the frequency response was evaluated, we examined the frequency response of L- and T-type calcium currents. These channels were first studied in isolation, and then inserted into the multi-compartment model.

Two-compartment, passive membrane model

The two-compartment model consisted of one compartment for the soma and one compartment for the terminal region (figure 1(B)) (see the Methods section). Each compartment contained a single resistor and capacitor in parallel. The two compartments were connected by a single resistor, representing current flow along the interior of the axon. Extracellular stimulation was simulated by placing a battery across the soma and terminal regions (V_{stim}). Because synaptic release results from depolarization of the synaptic terminals, we used the membrane potential in the terminals (V_{term}) as a measure of bipolar cell activation in response to sinusoidal extracellular stimulation (V_{stim}). The advantage of the two-compartment model is that it allowed an analytical solution to be derived with basic circuit analysis. We derived the circuit equations in the frequency domain because we were interested in the response to sinusoidal stimulation (Oppenheim *et al* 1996). The impedances of the soma, axon, and terminals are represented in the Laplace domain as follows:

$$Z_{soma} = R_{soma}/(1 + s R_{soma} C_{soma}) \quad (1)$$

$$Z_{axon} = R_{axon} \quad (2)$$

$$Z_{term} = R_{term}/(1 + s R_{term} C_{term}) \quad (3)$$

where s is the complex frequency. V_{term} was solved for using a voltage divider:

$$V_{term} = V_{stim}(Z_{term}/(Z_{term} + Z_{soma} + Z_{axon})). \quad (4)$$

Nominal values for resistance and capacitance for each compartment were derived from previous work (Oltegal *et al* 2009) (see the Methods section). With these parameter values, we computed the transfer function (V_{term}/V_{stim}) for frequencies ranging from 1 to 10^4 Hz (figure 1(C)). The sensitivity of the response (V_{term}) to the applied stimulus (V_{stim}) was nearly constant up to several hundred hertz and then declined steadily for increasing stimulus frequencies. Therefore, the relationship between the applied stimulus and the membrane potential in the terminals exhibits lowpass filtering characteristics. We defined cutoff frequency as the frequency at which the response is reduced by 3 dB from maximum; the cutoff frequency for the nominal parameter values was 895 Hz. This suggests that the passive membrane properties of the cell have little effect on the response out to relatively high frequencies.

There are at least ten different types of bipolar cells whose size and morphology vary considerably (Euler and Wassle 1995, Boycott and Wassle 1999, Wu *et al* 2000). To determine how these anatomical differences might influence the frequency response, we systematically varied each model

parameter and explored the effect on the transfer function. For example, the transfer function was computed for an axonal resistance (R_{axon}) value of nominal, one-half nominal, and twice nominal (figure 2(A)). As R_{axon} was increased, the cutoff frequency decreased. Interestingly, variations in R_{axon} had a negligible influence on the response to low-to-moderate frequencies ($<10^2$ Hz), suggesting that variations in intra-axonal resistance only affect the cutoff frequency.

To determine the range of cutoff frequencies arising from changes in the axonal resistance (R_{axon}), the cutoff frequency was computed for values of R_{axon} ranging from $1/8$ to $8\times$ its nominal value (figure 2(B)). This range of axonal resistance corresponds to a factor of 2 change in both axonal length and axonal diameter. For example, if the length of the axon is doubled and the diameter is halved, then the resistance of the intra-axonal current flow will increase by a factor of 8 (the change in cross-sectional area increased resistance by a factor of 4 and the change in length increased the resistance by a factor of 2). This range of parameters likely spans the range of bipolar cell morphology seen across bipolar cell types (see the Methods section). The cutoff frequency was found to decrease for increasing axonal resistance (i.e. longer, thinner axons), but remained relatively high (>117 Hz) even for the largest value of R_{axon} tested. In contrast, the cutoff frequency increased dramatically for decreasing axonal resistance (i.e. shorter, wider axons). Given that the cutoff frequency tends to plateau for high values of R_{axon} (figure 2(B)), it is likely that the cutoff frequency will remain relatively high for all anatomically realistic variations in axonal resistance.

Changes in the size of the soma or terminals will change both the resistance and capacitance of each compartment. Therefore, we first varied the resistance and capacitance independently in order to determine the individual contributions of each to the transfer function. Interestingly, varying the resistance of the soma (R_{soma}) or terminals (R_{term}) affected only the low-frequency portion (<10 Hz) of the transfer function, leaving the cutoff frequency unchanged (figures 3(A) and (B)). Changing the somatic or terminal resistance had opposing effects; increasing the somatic resistance caused a reduction in gain at low frequencies, while increasing the terminal resistance caused an increase in gain at low frequencies. The effect on gain was modest; in each case, changing the resistance by a factor of 2 caused a change in gain $\sim 15.2\%$ for stimulation at 1 Hz.

Changes in the capacitance of the somatic or terminal regions also altered the transfer function. For changes in the somatic capacitance, the effect was confined to the range of 10 – 10^3 Hz, while changes to the terminal capacitance affected all frequencies >10 Hz (figures 3(C) and (D)). In both cases, there was relatively little effect for frequencies <10 Hz. Changes in the capacitance of the soma or terminals had opposing effects; increasing the capacitance of the soma caused an increase in gain, while increasing the capacitance of the terminals had a decrease in gain.

Understanding how the resistance and capacitance influence the transfer function allowed the effects of anatomical changes (e.g. soma size) to be more easily understood. The effect of varying soma or terminal size was

performed by adjusting both the resistance and capacitance of a given compartment. For example, doubling the size of the soma was performed by increasing the capacitance by a factor of 2 and simultaneously decreasing the membrane resistance by a factor of 2. Increasing soma size produced an increase in gain at frequencies of $<10^3$ Hz, leaving higher frequencies relatively unaffected (figure 3(E)). Conversely, increasing the size of the terminals caused a reduction in gain across all frequencies (figure 3(F)).

Multi-compartment passive membrane model

While the two-compartment model has the advantage of allowing an analytical solution to be derived, it does not account for the complex morphological structure of a bipolar cell. Therefore, we examined the response properties of a morphologically realistic, multi-compartment bipolar cell (Oltedal *et al* 2009) (figures 4(A) and (B)). Each compartment was defined by a membrane conductance (g_{leak}) and capacitance (C_m), as well as by resistance to current flow along the interior of the cell (g_{intra}). The conductance g_{intra} was computed as a function of intra-cellular resistivity (ρ_i) (see the Methods section). The membrane potential at the terminals (V_{term}) was measured in response to sinusoidal stimulation delivered from an extracellular electrode (V_e) (see the Methods section). As with the two-compartment model, the multi-compartment model did not contain voltage-gated channels initially so that the contribution of the passive electrical properties of the membrane to the frequency response could be studied in isolation.

In general, the responses of the morphologically realistic bipolar cell model were similar to those obtained for the two-compartment model. The frequency response was lowpass with a cutoff frequency of 717 Hz for the nominal parameter values (figure 4(B)). Once again, the curve obtained using nominal parameter values is re-plotted in figures 5–7 to facilitate comparison (labeled as ‘Nominal’). As with the two-compartment model, varying the somatic or terminal membrane conductance only influenced the response to low frequencies (<10 Hz) (figures 5(A) and (B)), while varying the capacitance affected the response to frequencies >10 Hz (figures 5(C) and (D)). Likewise, varying the size of the soma or terminals in the multi-compartment model produced a nearly identical effect as that seen in the two-compartment model (figures 5(E) and (F) versus figures 3(E) and (F)). Unlike the two-compartment model, the axon of the multi-compartment model has a membrane with an associated conductance and capacitance. However, variations in the conductance or capacitance of the axonal membrane had little effect on the frequency response (figures 6(A) and (B)).

Examining the influence of intra-axonal resistance on the frequency response in the multi-compartment model was more complex than the corresponding analysis in the two-compartment model. This is because the intra-axonal resistance for the two-compartment model is defined by a single parameter, R_{axon} , while the intra-axonal resistance in the multi-compartment model was a function of axonal diameter, axonal length and the resistivity of the intracellular medium

(ρ_i). We examined the influence of each of these parameters on the frequency response. Changes to the intra-axonal resistivity influenced the cutoff frequency, but had little effect on gain (figure 6(C)). We measured the cutoff frequency as a function of intra-axonal resistivity (figure 6(D)), and in order to allow a direct comparison to the two-compartment model to be made, the results are plotted as a function of total intra-axonal resistance (not resistivity). We found that the dependence of cutoff frequency on intra-axonal resistance was nearly identical for the two models (compare figure 6(D) with figure 2(B)).

We next examined the effect of varying axonal diameter on the frequency response. Changes to axon diameter will affect the total membrane conductance and capacitance, as well as the resistance to intra-axonal current flow. However, since changes to the axonal membrane conductance and capacitance had little effect on the frequency response (figures 6(A) and (B)), we expected that changing the axonal diameter would produce results that were similar to those when the intra-axonal resistance was changed. This was found to be the case, as varying axonal diameter influenced the cutoff frequency, but had little effect on the response to low stimulus frequencies (figure 6(E)). Smaller axonal diameters resulted in increased resistance to intra-axonal current flow, producing a lower cutoff frequency.

We also explored how changes to axonal length affected the frequency response. In our model, changes to axonal length altered the distance between the axon terminals and the stimulating electrode. However, moving the terminals closer to the stimulating electrode would increase the sensitivity of the cell to the applied stimulus. Therefore, it was necessary to decouple the effects due to changing axonal length from those due to changing the position of the stimulating electrode. This was performed in a two-step process:

First, we measured the frequency response for variations in axonal length with the electrode fixed to a set distance (40 μm) from the terminals (figure 7(A)). Under these conditions, we found that increasing the length of the axon caused an increase in gain, as well as a decrease in cutoff frequency. Normalizing and overlaying the curves obtained for each axonal length revealed that longer axons are associated with lower cutoff frequencies (figure 7(B)). This finding is consistent with previous simulations that showed that increases in intra-axonal resistance resulted in a decrease in cutoff frequency (figure 6(D)). The increased gain for longer axons likely results from the larger spatial gradient in extracellular potential that exists across longer axons as compared to shorter axons.

Second, we held axonal length constant and measured the frequency response as the distance between the stimulating electrode and the terminals was varied (figure 7(C)). As expected, the sensitivity to stimulation was greatly increased when the distance between the stimulating electrode and the terminals was reduced. Normalizing and overlaying these responses reveals that electrode distance does not significantly affect cutoff frequency (figure 7(D)). Taken together, the results from figure 7 indicate that longer axons are associated with a decrease in cutoff frequency and an increase in

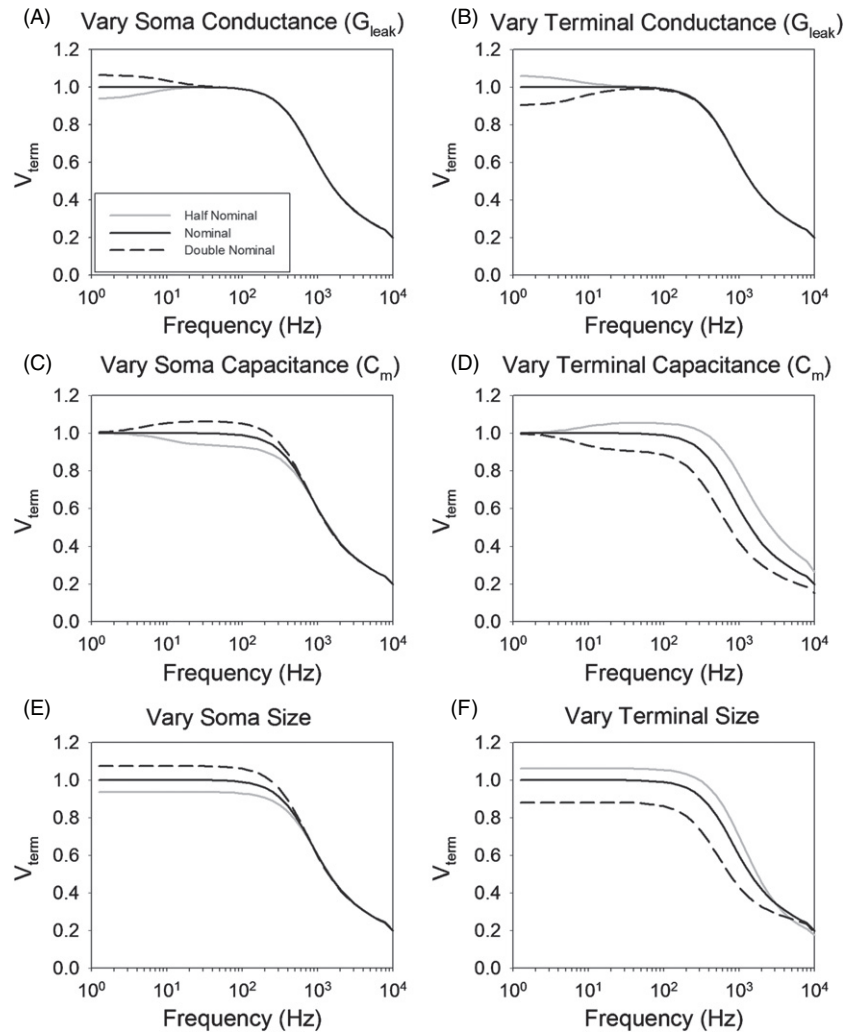


Figure 5. Effect of varying somatic and terminal membrane parameters on the frequency response of the multi-compartment model. The membrane potential in the terminals (V_{term}) in response to sinusoidal stimulation is shown for variations in the somatic (A) and terminal (B) membrane conductance (G_{leak}), as well as the somatic (C) and terminal (D) capacitance (C_m). The size of the soma (E) and terminals (F) was varied by scaling both conductance and capacitance (i.e. doubling the size of the soma is simulated by doubling both g_{leak} and C_m in all the soma compartments). For all plots, the nominal curve was normalized to unity and the other curves were scaled relative to this value (see the Methods section). The legend in panel A applies to all plots.

sensitivity to low stimulus frequencies. Conversely, changes to the distance between the bipolar cell and the stimulating electrode affect the response to all frequencies uniformly (i.e. does not alter cutoff frequency).

The frequency response of L- and T-type calcium channels

Synaptic release from bipolar cells is mediated by calcium entry to the terminals via L- and/or T-type calcium channels (Tachibana *et al* 1993, Pan *et al* 2001). These channels are voltage dependent, and equations that describe the relationship between membrane potential and the probability of opening (and thus calcium conductance) have been derived for L- and T-type channels in other types of neurons and were adopted for use in our model (see the Methods section) (De Schutter and Bower 1994, Benison *et al* 2001). The frequency-dependent response properties of these channels were examined by modulating voltage (V) sinusoidally across a range of frequencies and measuring the resulting current

(I_L and I_T) (figure 8(A)). Unlike the linear passive model, the gating equations are nonlinear, and therefore the frequency response may depend on the amplitude of the applied voltage.

The voltage was oscillated around a mean of -50 mV; this value was chosen to approximate the resting potential of bipolar cells (Ma *et al* 2005). In response to light, the fluctuations in bipolar cell membrane potential are thought to saturate near 15–25 mV (Nelson and Kolb 1983, Euler and Masland 2000). However, in response to electric stimulation, it is possible that much larger fluctuations in membrane potential could occur. Therefore, we examined the behavior of calcium channels for two ranges of voltage fluctuations: a physiologically realistic range (deviations of 2.5–20 mV from baseline) and a larger range that could potentially be induced by extracellular electric stimulation (deviations of 40–100 mV from baseline).

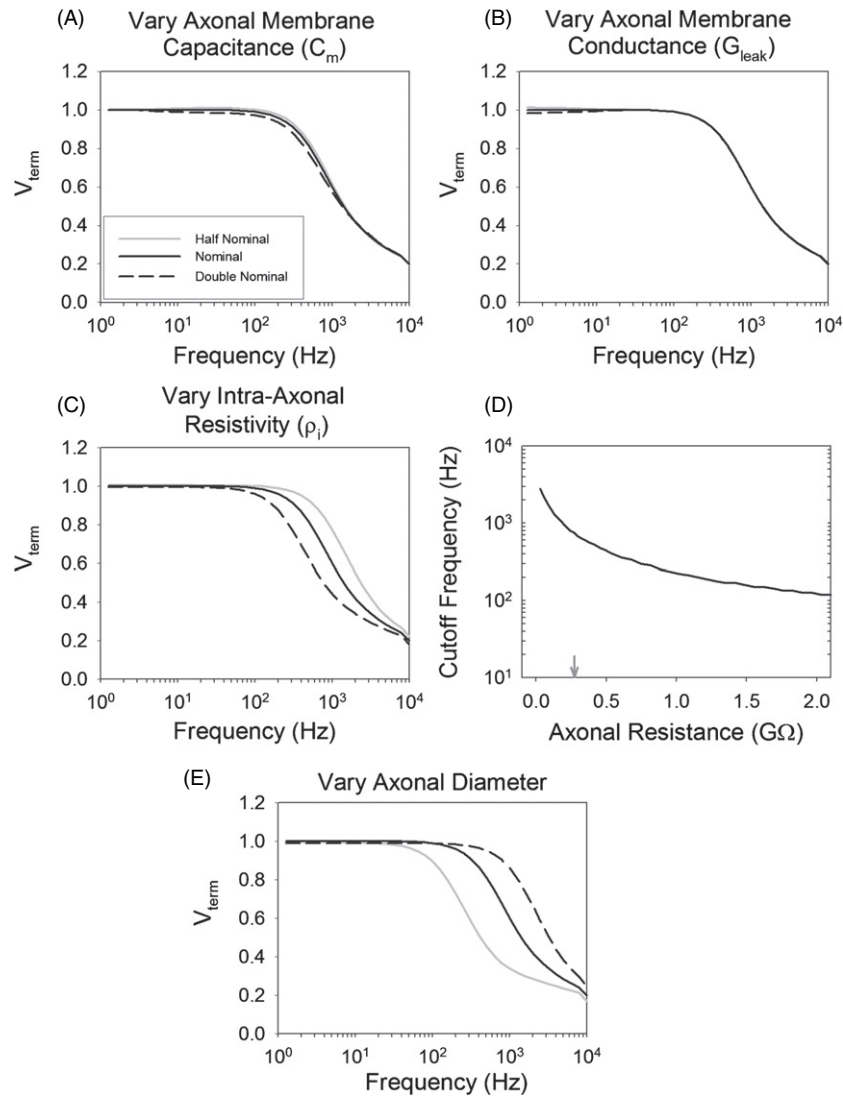


Figure 6. Changes in intra-axonal resistance alter the cutoff frequency in the multi-compartment model. The membrane potential in the terminals (V_{term}) is measured as a function of stimulus frequency for variations in axonal membrane capacitance (A) and conductance (B), axonal resistivity (C) and axonal diameter (E). The cutoff frequency is plotted as a function of total intra-axonal resistance (D). The arrow indicates the nominal resistance. For plots A–C and E, the nominal curve was normalized to unity and the other curves were scaled relative to this value (see the Methods section). The legend in panel A applies to panels (B), (C) and (E).

In response to voltage fluctuations of ≤ 20 mV, L-type calcium channels exhibited lowpass filtering characteristics, yielding larger currents at low frequencies than at high frequencies (figure 8(B)). Normalizing and overlaying these response curves revealed that the cutoff frequency decreased slightly as stimulus amplitude increased (figure 8(C)). Interestingly, once the range of voltage fluctuations exceeded ~ 40 mV, the shape of the frequency response changed from lowpass to bandpass (figure 8(D)). For voltage fluctuations > 40 mV, the response at low frequencies became saturated, while the response at moderate to high frequencies continued to increase. This can be seen more clearly by plotting the peak current as a function of stimulus voltage for two different frequencies (10 and 200 Hz) (figure 8(E)). Note that the maximal response currents achieved at a frequency of 200 Hz are nearly twice the maximal response at 10 Hz.

The cutoff frequency varied significantly as a function of stimulus voltage for L-type channels, exhibiting a parabolic shape with a minimum cutoff frequency of 65 Hz at ~ 34 mV (figure 8(F)). Note that in order to compare the cutoff frequencies for the lowpass and bandpass frequency responses, the cutoff frequency was always defined as the highest frequency at which the response was reduced by 3 dB (i.e. not defined as the peak of the frequency response). Taken together, these data suggest there are two separate modes of behavior for L-type calcium channels. For moderate fluctuations in voltage, the frequency response is lowpass, and the cutoff frequency decreases as voltage increases. For higher fluctuations in voltage, the frequency response becomes bandpass and the cutoff frequency increases with voltage.

As with the L-type channel, the frequency response of T-type channels was obtained by varying the voltage (V) sinusoidally and measuring the resulting current (I_T)

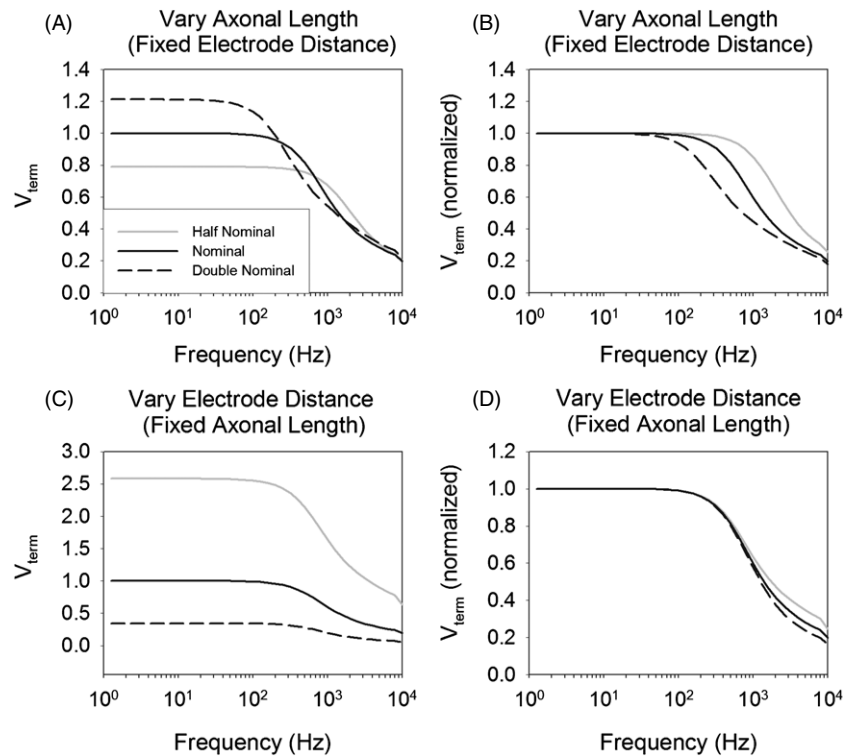


Figure 7. Effect of varying axonal length and electrode distance on the frequency response of the multi-compartment model. (A) Axonal length was changed to one-half and then twice that of nominal with the stimulating electrode at a fixed distance from the terminals ($40 \mu\text{m}$). (B) Each trace in panel A was normalized to unity and re-plotted to allow comparison of the cutoff frequency. (C) The distance of the stimulating electrode was changed to one-half and then twice that of the nominal value, while the length of the axon was held constant. (D) The traces in panel C were all normalized to unity and re-plotted. The legend in panel A applies to all plots. For plots A and C, the nominal curve was normalized to unity and the other curves were scaled relative to this value (see the Methods section).

(figure 9(A)). The frequency response of the T-type channels exhibited bandpass characteristics with a pronounced peak in sensitivity near 10 Hz (figure 9(B)). Normalizing and overlaying these response curves revealed that the general shape of the frequency response was maintained as voltage level was increased (figure 9(C)), although the peak shifted to slightly lower frequencies for higher voltage fluctuations (figure 9(D)). Currents through the T-type channel increased approximately linearly over the range of membrane potential levels tested for 200 Hz, whereas for 10 Hz stimulation, there was slight response compression for voltage fluctuations $>40 \text{ mV}$ (figure 9(E)). The frequency at which the response was maximal (i.e. peak frequency) varied with stimulus voltage, but always remained below 25 Hz (figure 9(F)).

Surprisingly, current continued to flow through T-type channels even for high stimulus frequencies (figures 9(B) and (D)). To explore why this occurred for T-type channels but not for L-type channels, we examined the activation variables of L- and T-type channels, as well as the inactivation variable of the T-type channel, across a range of stimulus frequencies (figure 10). The peak-to-peak value of $n(t)$ (the T-type activation variable) decreased as stimulus frequency was increased from 10 to 200 Hz, but the mean value of $n(t)$ was larger at 200 Hz than at 10 Hz (figure 10(A)). This was not the case for the L-type activation variable, $m(t)$, where increasing the frequency from 10 to 200 Hz caused a reduction in both the peak-to-peak and mean value of $m(t)$ (figure 10(B)). This

point was further illustrated by measuring peak-to-peak and mean values of the activation and inactivation variables for frequencies up to 1 kHz (figures 10(C) and (E)). Note that the mean value of the T-type activation variable increased and plateaued at a nonzero value for high stimulus frequencies (figure 10(C), bottom). For the stimulations in figure 10, the stimulus amplitude used was 40 mV, but similar behavior was observed for stimulus amplitudes ranging from 2.5 to 100 mV (data not shown).

Because T-type channels contain both activation and inactivation gating parameters, it is necessary for both to be non-zero in order for current to flow through the channel at high stimulus frequencies. As figure 10(C) indicates, the activation variable, $n(t)$, is much greater than zero (~ 0.85) for high stimulus frequencies. Although the mean inactivation variable, $h(t)$, decreases for increasing stimulus frequency (figure 10(E)), it plateaus at a nonzero value (~ 0.015). Therefore, the steady-state conductance is nonzero for high stimulus frequencies. This is further illustrated by comparing the scaling factors used to compute conductance for each channel: for T-type channels, this is the product of the activation and inactivation variables ($n(t) \times h(t)$), and for L-type channels, this is the square of the activation variable ($m^2(t)$) (figure 10(F)) (see the Methods section). Note that for T-type channels, this scaling factor plateaus for increasing stimulus frequency, while for L-type channels, the scaling factor continues to decrease for increasing frequency. Thus,

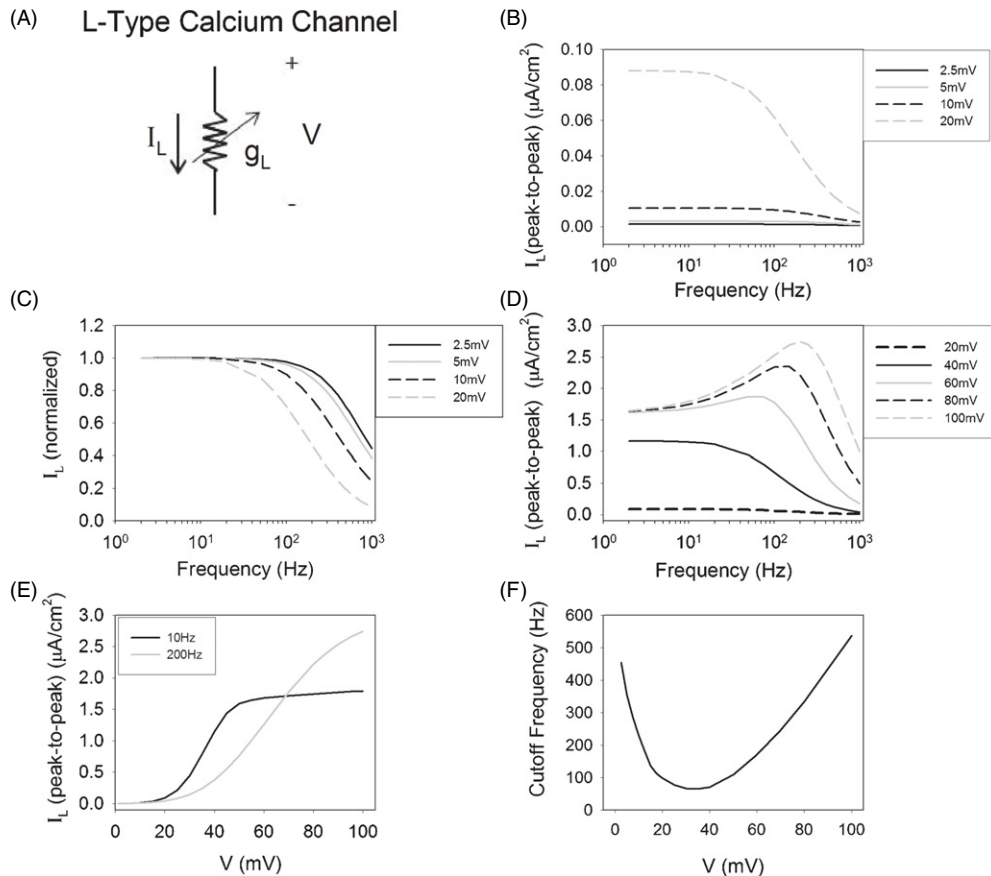


Figure 8. The frequency response of L-type calcium channels changes with stimulus amplitude. (A) Illustration of the model for the L-type calcium channel. The current, I_L , is measured in response to sinusoidal modulations in voltage (V), and g_L is related nonlinearly to voltage. (B) Peak-to-peak calcium current is measured as a function of frequency for voltage fluctuations ranging from 2.5 to 20 mV. (C) The traces in panel B were re-plotted after normalizing all curves to unity. (D) The same as in (B), but for fluctuations in voltage ranging from 20 to 100 mV. For clarity, the trace obtained for the 20 mV stimulus in panel B was re-plotted. (E) The peak-to-peak current is plotted as a function of stimulus voltage for 10 and 200 Hz. (F) The cutoff frequency is plotted as a function of stimulus amplitude.

our results suggest that T-type channels allow calcium current to flow for very rapid fluctuations in voltage, even though the channels themselves cannot open and close at such high rates. This is not true for L-type channels since the activation variable continued to decrease for increasing stimulus frequency.

Multi-compartment model with calcium channels

One of the original goals of this study was to understand why synaptic release from bipolar cells was elicited in response to extracellular sinusoidal stimulation at low frequencies (≤ 10 –25 Hz), but not for high frequencies (100 Hz) (Freeman *et al* 2010). Our results so far suggest that the lack of synaptic release of bipolar cells in response to 100 Hz stimulation was not likely to be the result of passive filtering by the bipolar cell membrane. In addition, the simulations with calcium channels suggest that calcium currents will be largest for low stimulus frequencies (tens of hertz). In order to make a direct comparison between the effects of calcium channel dynamics to those of passive membrane filtering, we inserted L- and T-type calcium channels into the terminal region of the multi-compartment model (figure 11(A)). Simulations were performed with both channel types inserted simultaneously,

but the results did not differ if the L- and T-type channels were inserted independently (data not shown).

The total membrane conductance for L- and T-type calcium channels in bipolar cells is not known, and therefore was set equal to the leak conductance ($g_{Lmax} = g_{Tmax} = g_{leak}$) (see the Methods section). With these conductance levels, we found that the frequency response of V_{term} did not change appreciably when the channels were added (figure 11(B)). This indicates that for these values of calcium conductance, the presence of the calcium channels did not affect the relationship between the applied stimulus and V_{term} . Although fluctuations in membrane potential may differ in the soma versus terminals, synaptic release takes place only in the terminals, and therefore we only inserted calcium channels into the terminals region. However, because the presence of the calcium channels does not affect the response of the membrane potential to stimulation, the presence of calcium channels in other sections of the bipolar cell (e.g. the soma) will not influence the variable of interest—the current through the calcium channels in the terminals.

We measured the current through L- and T-type calcium channels in order to infer the level of synaptic release in response to extracellular sinusoidal stimulation.

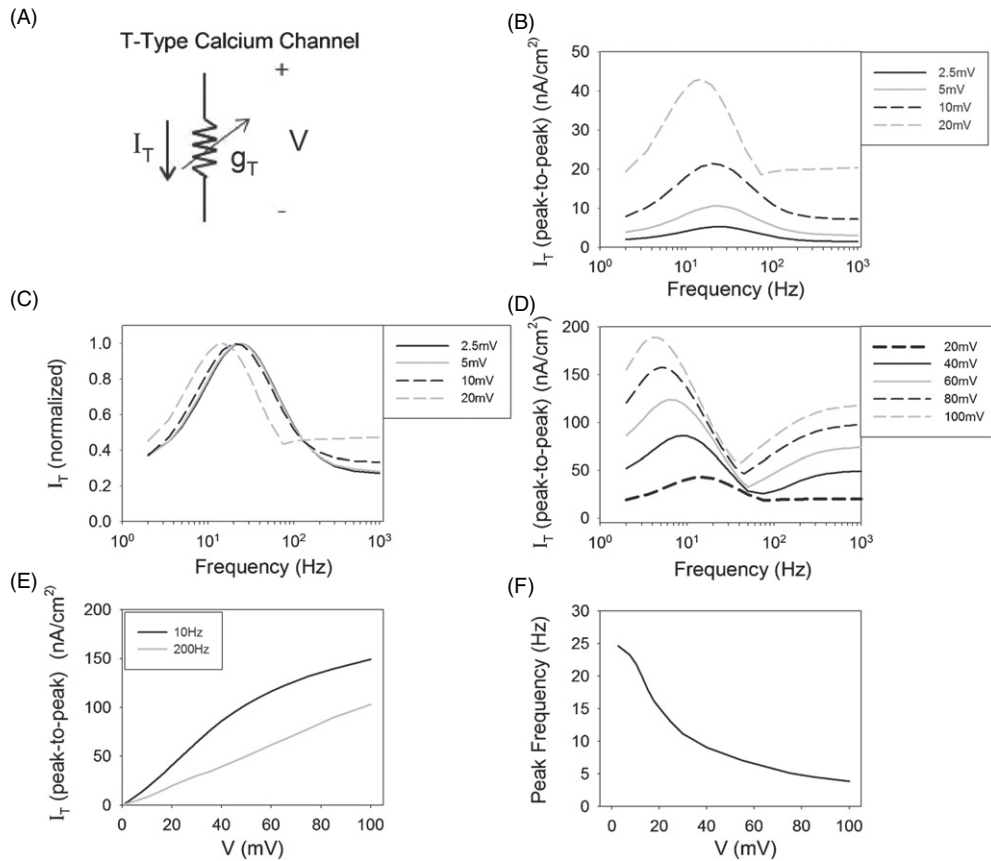


Figure 9. The frequency response of T-type calcium channels is bandpass. (A) Illustration of the model for the T-type calcium channel. The current, I_T , is measured in response to sinusoidal modulations in voltage (V), and g_T is related nonlinearly to voltage. (B) The peak-to-peak calcium current was measured as a function of frequency for fluctuations in voltage ranging from 2.5 to 20 mV. (C) Re-plotting the traces in panel B after normalizing all curves to unity. (D) The same as in (B), but for fluctuations in voltage ranging from 20 to 100 mV. For clarity, the trace obtained for the 20 mV stimulus in panel B was re-plotted. (E) The peak-to-peak current is plotted as a function of stimulus voltage for 10 and 200 Hz. (F) The frequency at which I_T is maximal as a function of stimulus amplitude.

Stimulus amplitudes were adjusted to produce modulations in membrane potential (V_{term}) in the range of 2.5–100 mV and the resulting L-type current (I_L) and T-type current (I_T) were measured (figures 12(A) and (B)). Considering the L-type channels first, we found that the shape of the frequency response went from lowpass to bandpass as stimulus amplitude increased. The cutoff frequency of the L-type current in the multi-compartment model was less than the cutoff frequency of the passive multi-compartment model (717 Hz for nominal parameters) for all stimulus amplitudes tested (figure 12(C)). Furthermore, the shape of the frequency response was identical to that obtained for the L-type calcium channel alone (figures 12(C) versus 8(F)). This suggests that the L-type channel mediated synaptic release from bipolar cells in response to electric stimulation is limited by the dynamics of L-type calcium channels and not by the passive properties of the membrane.

The frequency response for current through T-type calcium channels (I_T) in the multi-compartment model was found to be bandpass (figures 12(D) and (E)). The frequency yielding the largest response (i.e. the peak frequency) decreased for increasing stimulus amplitude, similar to the results obtained from T-type channels studied in isolation (figure 12(F), compare to figure 9(F)). As with the L-type

channels, the peak frequency of the T-type channel current was significantly less than the cutoff frequency of the passive membrane model for all stimulus amplitudes (maximum peak frequency = 22.4 Hz). Also, for stimulus frequencies up to ~200 Hz, the shape of the frequency response was similar to that obtained when studying the T-type channel in isolation (figure 12(E), compare to figure 9(D)). This suggests that for stimulus frequencies of <200 Hz, T-type channel mediated synaptic release is largely determined by the dynamics of T-type channels, and not by passive membrane properties. However, at higher stimulus frequencies (>200 Hz), the current through T-type channels in the multi-compartment model decreased steadily for increasing frequencies (figure 12(E)), while the current through T-type channels studied in isolation reached a plateau (figure 9(D)). This reduction in current at high stimulus frequencies is due to passive filtering of the membrane, preventing the membrane potential (V_{term}) from being modulated in response to rapid fluctuations of the stimulus (V_e). Therefore, the passive membrane properties may influence synaptic release for relatively high stimulus frequencies, while the response at frequencies of <200 Hz is largely determined by T-type channel dynamics.

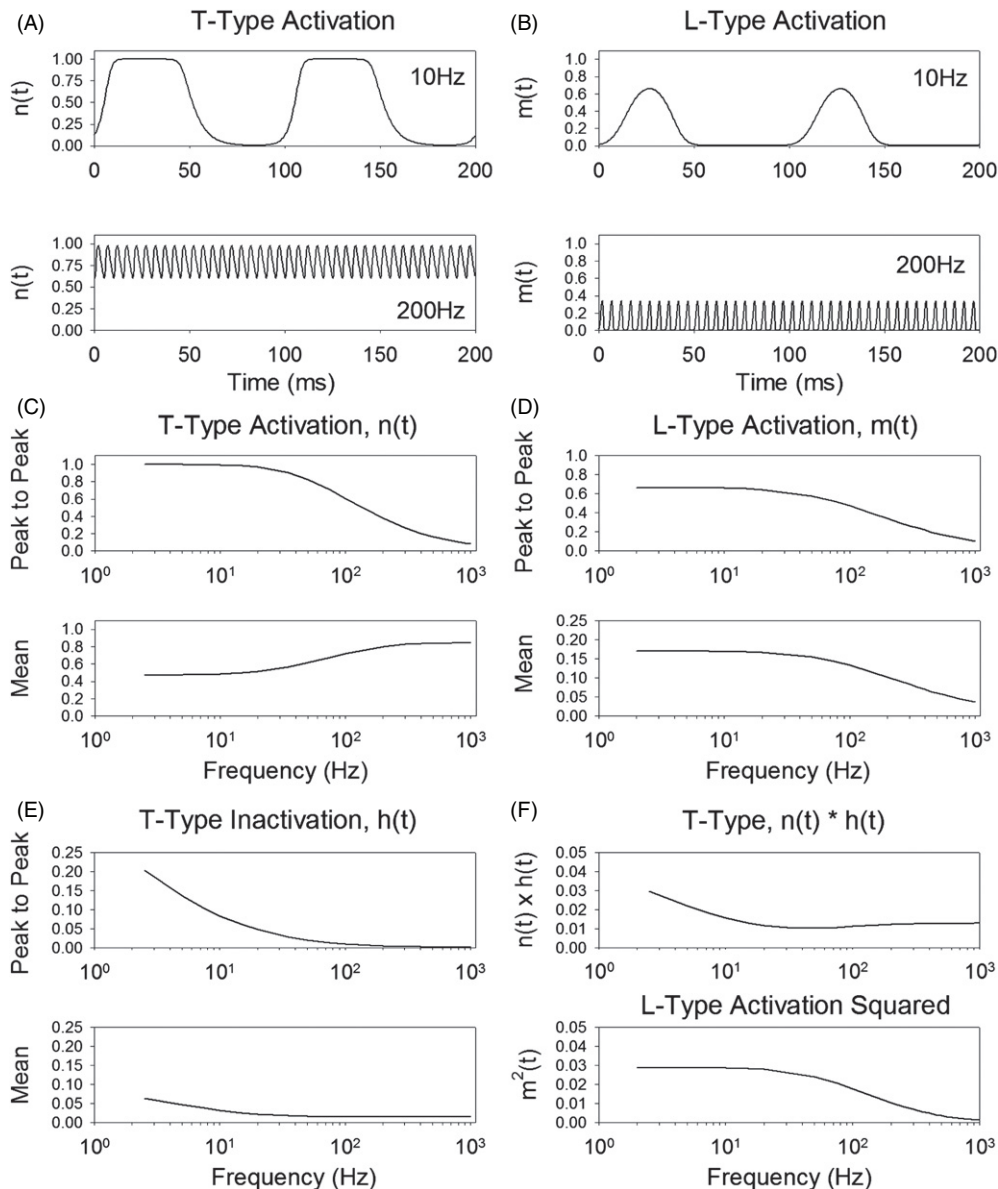


Figure 10. Effect of stimulus frequency on the activation/inactivation variables of L- and T-type calcium channels. (A) The T-type activation variable, $n(t)$, is plotted for stimulus frequencies of 10 (top) and 200 Hz (bottom). (B) Similar plots for the L-type activation variable, $m(t)$. (C)–(E) The peak-to-peak and mean response is shown as a function of frequency for the T-type activation variable $n(t)$, the L-type activation variable $m(t)$ and the T-type inactivation variable $h(t)$. (F) The scaling factors used to compute channel conductance are plotted for T-type channels ($n(t) \times h(t)$) (top) and L-type channels ($m^2(t)$) (bottom). The plots in (F) were calculated using the mean value of each gating variable (i.e. the lower plots in panels (C)–(E)). The stimulus amplitude was 40 mV in all cases.

Discussion

The ability to selectively target individual classes of neurons by varying stimulus frequency has considerable potential in retinal implants and neural prosthetics in general. A recent physiological study found that bipolar cells produced robust synaptic output in response to sinusoidal electric stimulation at frequencies of 10–25 Hz, but responded only weakly to 100 Hz stimulation (Freeman *et al* 2010). It is important to understand the physiological mechanisms underlying this frequency dependence as a step toward improving methods of selective activation. Using a morphologically realistic bipolar cell model, we provide evidence that the preferential response

of bipolar cells to low stimulus frequencies is largely due to the slow response dynamics of calcium channels, and not due to the passive electrical properties of the membrane.

Passive membrane model

Using both a two-compartment and a morphologically realistic, multi-compartment model, we found that passive filtering by the membrane was lowpass with a relatively high cutoff frequency. The cutoff frequencies for the two-compartment and multi-compartment models were 895 and 717 Hz, respectively—both significantly higher than the range of frequencies (10–25 Hz) that elicited bipolar-cell mediated synaptic responses in retinal ganglion cells (Freeman *et al*

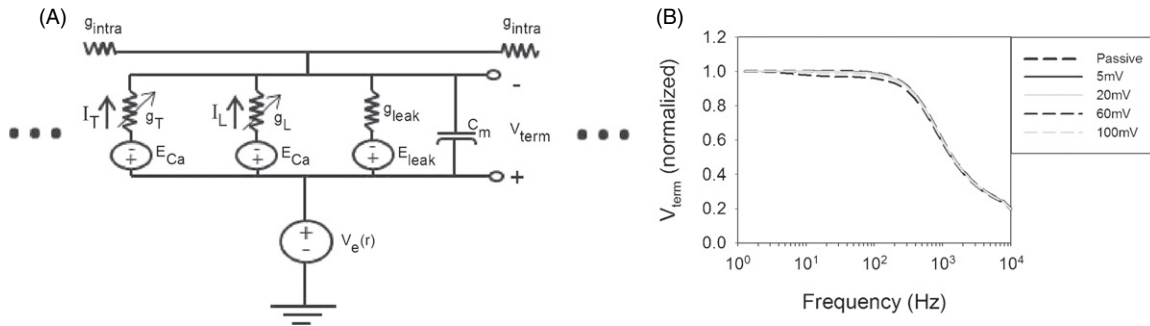


Figure 11. Incorporating calcium channels to the multi-compartment model does not affect the shape of the frequency response. (A) A single compartment of the multi-compartment model with calcium channels added. I_L and I_T represent current through the L- and T-type calcium channels, respectively. (B) The membrane potential in the terminals (V_{term}) was measured in response to extracellular sinusoidal stimulation ($V_e(r)$). The stimulus amplitude was adjusted to give peak modulations in V_{term} of 5, 20, 40 and 100 mV. The frequency response for each stimulus amplitude was normalized to unity and plotted along with the response of the passive model (i.e. no calcium channels).

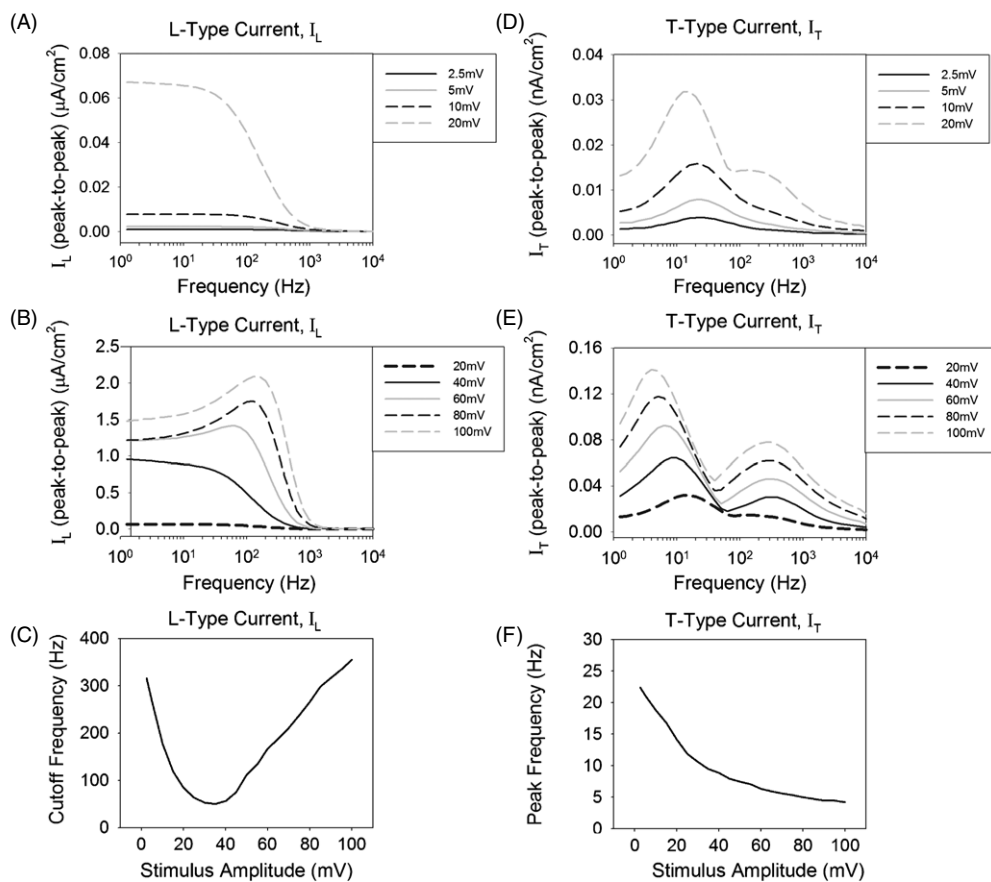


Figure 12. L- and T-type calcium channel dynamics limit the frequency response of calcium currents measured in the multi-compartment model. The peak-to-peak current through L-type (I_L) (A), (B) and T-type (I_T) (D), (E) channels in response to extracellular sinusoidal stimulation. The stimulus amplitude was adjusted to give peak modulations in membrane potential in the range of 2.5–100 mV, as indicated in the legends. The traces obtained for the 20 mV stimulus in panels (A) and (D) have been re-plotted in panels (B) and (E), respectively. The cutoff frequency of the L-type current (C) and the peak frequency of the T-type current (F) are plotted versus stimulus amplitude.

2010). This high cutoff frequency was preserved over a wide range of membrane parameters, cell sizes and cell morphologies. The lowest cutoff frequency observed for the passive membrane model was ~ 115 Hz, and this occurred only by decreasing axonal diameter to one-half nominal (resulting diameter = $0.36 \mu\text{m}$) and simultaneously increasing axonal length to double the nominal value (resulting length = $79.2 \mu\text{m}$) (figure 6(B)). These values of axonal length and

diameter are at the outer limits of those reported in anatomical studies (Euler and Wassle 1995, Tsukamoto *et al* 2001, Ghosh *et al* 2004, Oltedal *et al* 2009), suggesting that typical cutoff frequencies arising from the passive membrane properties of bipolar cells are likely to be significantly higher than 115 Hz.

The results of the passive membrane models (both the two-compartment and multi-compartment) are consistent with two recent modeling studies on retinal bipolar cells. One

study showed that in response to extracellular stimulation with voltage steps, the rise time of membrane potential was faster in bipolar cells with shorter axons, but the steady-state values of membrane potential were lower (Gerhardt *et al* 2010). This is consistent with our finding that bipolar cells with shorter axons had higher cutoff frequencies and reduced gain (figures 7(A) and (B)). Another computational study modulated membrane potential at the bipolar cell soma sinusoidally (voltage-clamp) and measured the resulting membrane potential at the terminals (Oltedal *et al* 2009). Their results indicated lowpass filtering as a result of the passive propagation of signals from the bipolar cell soma to the terminals. They found that the cutoff frequency increased with axonal diameter, while increasing the axonal length or intra-axonal resistivity resulted in a lower cutoff frequency. Also, they found cutoff frequencies that were relatively high, ranging from 300 to 1800 Hz. These findings are consistent with our results showing that the passive membrane properties of bipolar cells attenuate the response to extracellular stimulation only at relatively high frequencies.

An intuitive explanation as to why the cutoff frequency was highly dependent on intra-axonal resistance can be obtained by analyzing the circuit of the two-compartment model (figure 1(B)). For the nominal bipolar cell, the intra-axonal resistance ($R_{\text{axon}} = 0.27 \text{ G}\Omega$) was much less than the membrane resistance of the soma ($R_{\text{soma}} = 5.98 \text{ G}\Omega$) or terminals ($R_{\text{term}} = 27.9 \text{ G}\Omega$). For low-frequency stimulation, the impedance of the capacitors is extremely large (approaching infinite impedance for dc), and therefore the relationship between the stimulus (V_{stim}) and the membrane potential in the terminals (V_{term}) can be approximated by a simple voltage divider between the terminal resistor (R_{term}) and the other two resistors ($R_{\text{soma}} + R_{\text{axon}}$). But since $R_{\text{axon}} \ll R_{\text{soma}}$, the effect of changing R_{axon} is negligible. As the stimulus frequency is increased, the impedance of the capacitors becomes smaller, leading to a smaller impedance of both the soma and terminal compartments. As a result, the relative amount of voltage dropped across R_{axon} becomes larger, and changes in the value of R_{axon} are no longer negligible. Therefore, changes in R_{axon} will alter the cutoff frequency of the circuit, but only for stimulation at high frequencies.

Implications for selective activation of individual types of bipolar cells

Bipolar cells can be broadly categorized as either ON or OFF based on the polarity of their response to light (Werblin and Dowling 1969). There are anatomical differences between these cell classes; ON cells have longer axonal processes and ramify within the inner portion of the inner plexiform layer (IPL), while OFF cells have shorter processes and ramify within the outer portion of the IPL (Famiglietti and Kolb 1976). The models simulated here allowed us to explore whether the correct choice of stimulus frequency could facilitate the preferential activation of either ON or OFF bipolar cells.

The shorter axonal length of OFF bipolar cells corresponds to a lower intra-axonal resistance as compared to ON bipolar cells. This results in a higher cutoff frequency for

OFF cells relative to ON cells, yielding a range of frequencies over which OFF bipolar cells could potentially be depolarized while producing little or no depolarization in ON bipolar cells (figure 7(B)). However, longer axons (i.e. those in ON bipolar cells) also have a significantly larger gain than shorter axons (figure 7(A)). Therefore, high-frequency stimulation (e.g. 500 Hz) could produce a response of similar magnitude in ON and OFF cells, even though the ON cell response is attenuated at this frequency. Therefore, despite having a larger cutoff frequency, it may not be possible to preferentially activate OFF cells at high frequencies. Furthermore, our results suggest that calcium channel dynamics would limit the ability to produce synaptic output for such rapid fluctuations in membrane potential (figure 12).

Another possibility to consider is whether ON cells can be preferentially activated for low to moderate stimulus frequencies. This is because (1) longer axons have a higher sensitivity than shorter axons at these stimulus frequencies (figure 7(A)) and (2) the terminals of ON bipolar cells are slightly closer to the stimulating electrode than those of OFF bipolar cells (at least for epi-retinal stimulation). If we assume that the length of the axons in ON versus OFF bipolar cells differs by a factor of 2, then the results from figure 7(A) suggest that ON cells will be about $\sim 20\%$ more sensitive than OFF cells. The shorter distance between the stimulating electrode and ON bipolar cell terminals may further facilitate preferential activation of ON cells, but this will depend critically on the distance between the electrode and the inner surface of the retina. For example, in chronic retinal implants, the reported distance between a given electrode and the inner retinal surface is thought to range from 100 to 1000 μm (de Balthasar *et al* 2008). Because the human IPL is $\sim 40 \mu\text{m}$ thick (Kolb and Dekorver 1991), electrodes that are approximately 100 μm from the inner retinal surface would be significantly closer to the innermost portion of the IPL (and thus ON bipolar cell terminals), potentially allowing preferential activation of ON cells. In contrast, electrodes that are 1000 μm from the retina would effectively be at the same distance from the terminals of ON and OFF bipolar cells, making such preferential activation unlikely. The development of penetrating electrodes that allow electrodes to be positioned at specific depths within the retina may improve the ability to preferentially activate ON versus OFF bipolar cells (Palanker *et al* 2005, Winter *et al* 2007).

The expression of T- and L-type calcium channels varies across bipolar cells. While some bipolar cells display both L- and T-type currents, other express primarily L- or T-type currents (Hu *et al* 2009). These differences may serve as a basis for selective activation of individual types of bipolar cells using sinusoidal stimulation. For example, T-type channels responded only to relatively low frequencies ($< 25 \text{ Hz}$), while L-type channels responded to low and moderate frequencies (cutoff frequency ranging from 65 to 500 Hz). Thus, in response to stimulation at 60 Hz, only the L-type channels will open and allow calcium to flow into the cell, producing synaptic release only from those bipolar cells that express L-type channels. This approach would be most beneficial if the expression of L- or T-type channels were correlated to

specific physiological sub-types of bipolar cells; it is unknown whether this is the case (Awatramani and Slaughter 2000, Euler and Masland 2000, Hu *et al* 2009). However, recent work showed that there is a differential expression of T-type calcium channels in ON versus OFF ganglion cells (Margolis *et al* 2010), raising the possibility that cell-type specific expression patterns may also exist in bipolar cells.

Calcium currents in response to high-frequency stimulation

Our results suggest that the relatively slow kinetics of L- and T-type calcium channels may limit the ability of bipolar cells to initiate synaptic release for rapid fluctuations in membrane potential. However, there are two exceptions where synaptic release for high-frequency stimulation may be possible. First, the cutoff frequency for L-type channels increases for larger membrane potential fluctuations. Therefore, it may be possible to elicit L-type calcium currents if the membrane potential can be modulated by relatively large amounts (i.e. beyond the normal physiological range of ~ 15 – 25 mV) (Nelson and Kolb 1983, Euler and Masland 2000). However, an estimate of the maximum level of membrane depolarization that is possible with extracellular stimulation has not been reported. Second, although T-type channels respond optimally at low frequencies (~ 5 – 25 Hz), our results suggest that the steady-state conductance is non-zero for rapid modulations in membrane potential (figures 9(B)–(D)). Therefore, high-frequency stimulation may elicit currents through T-type channels even though the channels themselves do not open and close at the stimulus frequency. Importantly, this feature was not specific to the T-type model being employed since the high-frequency plateau of the frequency response was observed in both models we tested (Huguenard and McCormick 1992, De Schutter and Bower 1994) (supplementary figure 1 available at stacks.iop.org/JNE/8/046005/mmedia). It will be necessary to determine if T-type channels exhibit similar behavior under physiological conditions, or whether this effect is an artifact of the equations used to describe T-type channel behavior. Also, even if it is possible to elicit L- or T-type calcium currents at relatively high stimulus frequencies, the relationship between calcium influx and vesicle release is not instantaneous, but occurs with a time constant of ~ 1.1 ms (Oltedal and Hartveit 2010). Therefore, the release of synaptic vesicles will be attenuated for calcium currents oscillating faster than ~ 900 Hz.

Effects of calcium conductance and other voltage-gated ion channels

The total calcium channel conductance in bipolar cells has not been reported. In preliminary studies, we used whole-cell simulations of the multi-compartment model to determine the value of L-type calcium conductance that would yield currents similar in magnitude to those reported physiologically (Protti and Llano 1998) (data not shown). We estimated that the L-type conductance was ~ 5 mS cm^{-2} , similar in magnitude to the calcium conductance estimated in ganglion cells (~ 1 mS cm^{-2}) (Fohlmeister and Miller 1997), but significantly larger than the leak conductance (0.048 mS cm^{-2}). In simulations

for L-type channels, we found that if the calcium channel conductance was set to be larger than the leak conductance, then this resulted in a positive feedback effect: depolarization of the membrane caused L-type channels to open, and this caused more depolarization, and so on, until all channels were open and the membrane potential rested at the calcium reversal potential ($E_{\text{Ca}} = +45$ mV). We avoided this positive feedback effect by setting calcium channel conductance to be equal to the leak conductance—at this level, the opening/closing of calcium channels did not affect the relationship between the applied stimulus and the resulting modulations in membrane potential (figure 11(B)). Note that such positive feedback was not a concern for T-type channels because these channels inactivate at depolarized potentials, allowing the resting potential to return to the leakage reversal potential (E_{leak}).

Although regenerative activity of voltage-gated calcium channels has been shown to produce depolarization in bipolar cells (Protti *et al* 2000, Ma and Pan 2003), the membrane potential is quickly returned to rest (-40 to -50 mV) as a result of the activation of other voltage-gated ion channels (e.g. potassium) (Protti *et al* 2000). We chose not to incorporate other voltage-gated channels in the multi-compartment model for two reasons. First, the inclusion of such channels would make it difficult to separate the effects of passive membrane filtering and calcium channel dynamics from those of other channels. In particular, the continual opening and closing of both voltage-gated sodium and potassium channels would alter membrane conductance, and this would affect the relationship between the applied stimulus and the bipolar cell membrane potential. Second, the expression pattern of these other channels across different types of bipolar cells is not fully understood. For example, voltage-dependent potassium currents have been found to differ between rod bipolar and cone bipolar cells, as well as between different types of cone bipolar cells (Hu and Pan 2002). Similarly, voltage-gated sodium currents have been reported, but only in a subset of bipolar cells (Pan and Hu 2000). Therefore, inclusion of these channels into the model would require new assumptions as to the types and densities of these channels.

Implications for the temporal resolution of prosthetic vision

Ganglion cell spiking can be elicited through activation of presynaptic bipolar cells; this is referred to as indirect activation. In response to repetitive stimulation with pulses, the ganglion cell response to the first pulse is robust, but the response to subsequent pulses is greatly desensitized (Jensen and Rizzo 2007, Freeman and Fried 2011). Such desensitization has been reported for pulse rates as low as 2 Hz and severely limits the ability to control the temporal pattern of ganglion cell spiking elicited through the synaptic network. However, our results suggest that L- and T-type calcium channels can respond to frequencies of tens or hundreds of hertz (figures 8 and 9). Therefore, it is unlikely that calcium channel dynamics are responsible for the desensitization observed physiologically. If such a desensitization mechanism could be avoided, then it is possible that the indirect response

of ganglion cells will be limited by the slow kinetics of L- and T-type calcium channels at high stimulus frequencies. It is important to note that the influx of calcium into the cell can initiate a wide range of secondary processes, one or more of which could alter the sensitivity to ongoing stimulation.

Acknowledgments

We would like to thank Zhuo-Hua Pan and Donald Eddington for helpful input during the preparation of the manuscript. This work was supported by the Department of Veterans Affairs (CDA-1 to DF, CDA-2 to SK and 1I01RX000350-01A1 to SF) from (DF, SK) and the National Eye Institute (R01 EY-019967-01 to SF).

References

- Ahuja A K, Dorn J D, Caspi A, McMahon M J, Dagnelie G, daCruz L, Stanga P, Humayun M S and Greenberg R J 2010 Blind subjects implanted with the Argus II retinal prosthesis are able to improve performance in a spatial-motor task *Br. J. Ophthalmol.* **95** 539–43
- Awatramani G B and Slaughter M M 2000 Origin of the transient and sustained responses in ganglion cells of the retina *J. Neurosci.* **20** 7087–95
- Benison G, Keizer J, Chalupa L M and Robinson D W 2001 Modeling temporal behavior of postnatal cat retinal ganglion cells *J. Theor. Biol.* **210** 187–99
- Boinagrov D, Loudin J and Palanker D 2010 Strength–duration relationship for extracellular neural stimulation: numerical and analytical models *J. Neurophysiol.* **104** 2236–48
- Boycott B and Wässle H 1999 Parallel processing in the mammalian retina: the Proctor Lecture *Invest. Ophthalmol. Vis. Sci.* **40** 1313–27
- Caminos E, Velasco A, Jarrin M, Lillo C, Jimeno D, Aijon J and Lara J M 2000 A comparative study of protein kinase C-like immunoreactive cells in the retina *Brain Behav. Evol.* **56** 330–9
- Chader G J, Weiland J and Humayun M S 2009 Artificial vision: needs, functioning, and testing of a retinal electronic prosthesis *Prog. Brain Res.* **175** 317–32
- Coleman P A and Miller R F 1989 Measurement of passive membrane parameters with whole-cell recordings from neurons in the intact amphibian retina *J. Neurophysiol.* **61** 218–30
- de Balthasar C *et al* 2008 Factors affecting perceptual thresholds in epiretinal prostheses *Invest. Ophthalmol. Vis. Sci.* **49** 2303–14
- De Schutter E and Bower J M 1994 An active membrane model of the cerebellar Purkinje Cell: I. Simulation of current clamps in slice *J. Neurophysiol.* **71** 375–400
- Euler T and Masland R H 2000 Light-evoked responses of bipolar cells in a mammalian retina *J. Neurophysiol.* **83** 1817–29
- Euler T and Wässle H 1995 Immunocytochemical identification of cone bipolar cells in the rat retina *J. Comp. Neurol.* **361** 461–78
- Famiglietti E V and Kolb H 1976 Structural basis for ON- and OFF-center responses in retinal ganglion cells *Science* **194** 193–5
- Field G D and Chichilnisky E J 2007 Information processing in the primate retina: circuitry and coding *Annu. Rev. Neurosci.* **30** 1–30
- Fohlmeister J F and Miller R F 1997 Impulse encoding mechanisms of ganglion cells in tiger salamander retina *J. Neurophysiol.* **78** 1935–47
- Freeman D K, Eddington D K, Rizzo J F III and Fried S I 2010 Selective activation of neuronal targets with sinusoidal electric stimulation *J. Neurophysiol.* **104** 2778–91
- Freeman D K and Fried S I 2011 Multiple components of ganglion cell desensitization in response to prosthetic stimulation *J. Neural Eng.* **8**
- Freeman D K, Rizzo J F III and Fried S I 2011 Encoding visual information in retinal ganglion cells with prosthetic stimulation *J. Neural Eng.* at press
- Fried S I, Hsueh H A and Werblin F S 2006 A method for generating precise temporal patterns of retinal spiking using prosthetic stimulation *J. Neurophysiol.* **95** 970–8
- Gerhardt M, Alderman J and Stett A 2010 Electric field stimulation of bipolar cells in a degenerated retina—a theoretical study *IEEE Trans. Neural Syst. Rehabil. Eng.* **18** 1–10
- Ghosh K K, Bujan S, Haverkamp S, Feigenspan A and Wässle H 2004 Types of bipolar cells in the mouse retina *J. Comp. Neurol.* **469** 70–82
- Gollisch T and Meister M 2010 Eye smarter than scientists believed: neural computations in circuits of the retina *Neuron* **65** 150–64
- Greenberg R J, Velte T J, Humayun M S, Scarlatis G N and de Juan E Jr 1999 A computational model of electrical stimulation of the retinal ganglion cell *IEEE Trans. Biomed. Eng.* **46** 505–14
- Hartveit E 1999 Reciprocal synaptic interactions between rod bipolar cells and amacrine cells in the rat retina *J. Neurophysiol.* **81** 2923–36
- Hines M 1993 NEURON—a program for simulation of nerve equations *Neural Systems: Analysis and Modeling* (Norwell, MA: Kluwer)
- Hodgkin A L and Huxley A F 1952 A quantitative description of membrane current and its application to conduction and excitation in nerve *J. Physiol.* **117** 500–44
- Hu C, Bi A and Pan Z H 2009 Differential expression of three T-type calcium channels in retinal bipolar cells in rats *Vis. Neurosci.* **26** 177–87
- Hu H J and Pan Z H 2002 Differential expression of K⁺ currents in mammalian retinal bipolar cells *Vis. Neurosci.* **19** 163–73
- Huguenard J R and McCormick D A 1992 Simulation of the currents involved in rhythmic oscillations in thalamic relay neurons *J. Neurophysiol.* **68** 1373–83
- Jensen R J and Rizzo J F III 2007 Responses of ganglion cells to repetitive electrical stimulation of the retina *J. Neural Eng.* **4** S1–6
- Jensen R J, Ziv O R and Rizzo J F 2005a Responses of rabbit retinal ganglion cells to electrical stimulation with an epiretinal electrode *J. Neural Eng.* **2** S16–21
- Jensen R J, Ziv O R and Rizzo J F III 2005b Thresholds for activation of rabbit retinal ganglion cells with relatively large, extracellular microelectrodes *Invest. Ophthalmol. Vis. Sci.* **46** 1486–96
- Kaneko A, Pinto L H and Tachibana M 1989 Transient calcium current of retinal bipolar cells of mouse *J. Physiol.* **410** 613–29
- Kolb H and Dekorver L 1991 Midget ganglion cells of the parafovea of the human retina: a study by electron microscopy and serial section reconstructions *J. Comp. Neurol.* **303** 617–36
- Ma Y P and Pan Z H 2003 Spontaneous regenerative activity in mammalian retinal bipolar cells: roles of multiple subtypes of voltage-dependent Ca²⁺ channels *Vis. Neurosci.* **20** 131–9
- Ma Y P, Cui J and Pan Z H 2005 Heterogeneous expression of voltage-dependent Na⁺ and K⁺ channels in mammalian retinal bipolar cells *Vis. Neurosci.* **22** 119–33
- Margalit E and Thoreson W B 2006 Inner retinal mechanisms engaged by retinal electrical stimulation *Invest. Ophthalmol. Vis. Sci.* **47** 2606–12
- Margolis D J, Gartland A J, Euler T and Detwiler P B 2010 Dendritic calcium signaling in ON and OFF mouse retinal ganglion cells *J. Neurosci.* **30** 7127–38

- Margolis D J, Newkirk G, Euler T and Detwiler P B 2008 Functional stability of retinal ganglion cells after degeneration-induced changes in synaptic input *J. Neurosci.* **28** 6526–36
- Mazzoni F, Novelli E and Strettoi E 2008 Retinal ganglion cells survive and maintain normal dendritic morphology in a mouse model of inherited photoreceptor degeneration *J. Neurosci.* **28** 14282–92
- McCormick D A and Huguenard J R 1992 A model of the electrophysiological properties of thalamocortical relay neurons *J. Neurophysiol.* **68** 1384–400
- McIntyre C C and Grill W M 1998 Sensitivity analysis of a model of mammalian neural membrane *Biol. Cybern.* **79** 29–37
- McNeal D R 1976 Analysis of a model for excitation of myelinated nerve *IEEE Trans. Biomed. Eng.* **23** 329–37
- Mennerick S, Zenisek D and Matthews G 1997 Static and dynamic membrane properties of large-terminal bipolar cells from goldfish retina: experimental test of a compartmental model *J. Neurophysiol.* **78** 51–62
- Nelson R and Kolb H 1983 Synaptic patterns and response properties of bipolar and ganglion cells in the cat retina *Vis. Res.* **23** 1183–95
- Olstedal L and Hartveit E 2010 Transient release kinetics of rod bipolar cells revealed by capacitance measurements of exocytosis from axon terminals in rat retinal slices *J. Physiol.* **588** 1469–87
- Olstedal L, Morkve S H, Veruki M L and Hartveit E 2007 Patch-clamp investigations and compartmental modeling of rod bipolar axon terminals in an *in vitro* thin-slice preparation of the mammalian retina *J. Neurophysiol.* **97** 1171–87
- Olstedal L, Veruki M L and Hartveit E 2009 Passive membrane properties and electrotonic signal processing in retinal rod bipolar cells *J. Physiol.* **587** 829–49
- Oppenheim A V, Willsky A S and Nawab S H 1996 *Signals and Systems* 2nd edn (Englewood Cliffs, NJ: Prentice-Hall)
- Palanker D, Vankov A, Huie P and Baccus S 2005 Design of a high-resolution optoelectronic retinal prosthesis *J. Neural Eng.* **2** S105–20
- Pan Z H 2000 Differential expression of high- and two types of low-voltage-activated calcium currents in rod and cone bipolar cells of the rat retina *J. Neurophysiol.* **83** 513–27
- Pan Z H and Hu H J 2000 Voltage-dependent Na⁺ currents in mammalian retinal cone bipolar cells *J. Neurophysiol.* **84** 2564–71
- Pan Z H, Hu H J, Perring P and Andrade R 2001 T-type Ca²⁺ channels mediate neurotransmitter release in retinal bipolar cells *Neuron* **32** 89–98
- Protti D A, Flores-Herr N and von Gersdorff H 2000 Light evokes Ca²⁺ spikes in the axon terminal of a retinal bipolar cell *Neuron* **25** 215–27
- Protti D A and Llano I 1998 Calcium currents and calcium signaling in rod bipolar cells of rat retinal slices *J. Neurosci.* **18** 3715–24
- Rattay F 1998 Analysis of the electrical excitation of CNS neurons *IEEE Trans. Biomed. Eng.* **45** 766–72
- Rizzo J F III, Wyatt J, Loewenstein J, Kelly S and Shire D 2003 Perceptual efficacy of electrical stimulation of human retina with a microelectrode array during short-term surgical trials *Invest. Ophthalmol. Vis. Sci.* **44** 5362–9
- Sekirnjak C, Hottowy P, Sher A, Dabrowski W, Litke A M and Chichilnisky E J 2006 Electrical stimulation of mammalian retinal ganglion cells with multielectrode arrays *J. Neurophysiol.* **95** 3311–27
- Stett A, Mai A and Herrmann T 2007 Retinal charge sensitivity and spatial discrimination obtainable by subretinal implants: key lessons learned from isolated chicken retina *J. Neural Eng.* **4** S7–16
- Strettoi E, Pignatelli V, Rossi C, Porciatti V and Falsini B 2003 Remodeling of second-order neurons in the retina of rd/rd mutant mice *Vis. Res.* **43** 867–77
- Tachibana M, Okada T, Arimura T, Kobayashi K and Piccolino M 1993 Dihydropyridine-sensitive calcium current mediates neurotransmitter release from bipolar cells in the goldfish retina *J. Neurosci.* **707** 359–61
- Tsai D, Morley J W, Suaning G J and Lovell N H 2009 Direct activation and temporal response properties of rabbit retinal ganglion cells following subretinal stimulation *J. Neurophysiol.* **102** 2982–93
- Tsukamoto Y, Morigiwa K, Ueda M and Sterling P 2001 Microcircuits for night vision in mouse retina *J. Neurosci.* **21** 8616–23
- von Gersdorff H and Matthews G 1996 Calcium-dependent inactivation of calcium current in synaptic terminals of retinal bipolar neurons *J. Neurosci.* **16** 115–22
- Weiland J D, Liu W and Humayun M S 2004 Retinal prosthesis *Annu. Rev. Biomed. Eng.* **7** 361–401
- Werblin F S and Dowling J E 1969 Organization of the retina of mudpuppy, *necturus maculosus*: II. Intracellular recording *J. Neurophysiol.* **32** 339–55
- Winter J O, Cogan S F and Rizzo J F III 2007 Retinal prostheses: current challenges and future outlook *J. Biomater. Sci., Polym. Edn* **18** 1031–55
- Wu S M, Gao F and Maple B R 2000 Functional architecture of synapses in the inner retina: segregation of visual signals by stratification of bipolar cell axon terminals *J. Neurosci.* **20** 4462–70
- Zrenner E 2002 Will retinal implants restore vision? *Science* **295** 1022–5
- Zrenner E *et al* 2010 Subretinal electronic chips allow blind patients to read letters and combine them into words *Proc. R. Soc. Biol. Sci.* doi:10.1098/rspb.2010.1747